Electronic Supplementary Material (ESI) for Lab on a Chip.
This journal is © The Royal Society of Chemistry 2023

Supplementary Material

Ultrasonic spectroscopy of sessile droplets coupled to optomechanical sensors

K. G. Scheuer[a], F. B. Romero[b], G. J. Hornig[b], R. G. DeCorby[b*]

[a.] Ultracoustics Technologies Ltd., Sherwood Park, AB, Canada T8A 3H5

[b.] ECE Department, University of Alberta, 9211-116 St. NW, Edmonton, AB, Canada, T6G 1H9

*rdecorby@ualberta.ca

1 Experimental measurement system

The measurement system consisted of an optical reflection readout scheme similar to that described in previous work [1-3]. A telecom-band laser was tuned to the fundamental cavity resonance of a particular device and fiber-coupled into an optical circulator with SMF-28 fiber. The laser signal was collimated and focused through an objective lens at the second port of the circulator and aligned to the device using an infrared camera (Raptor Photonics Ninox 640). Light reflected from the device was passed back through the objective lens and collimator and back into the optical circulator where it was fiber coupled directly into a photodetector. A full schematic of the measurement system is shown in Fig. S.1 along with a cross-sectional schematic of a buckled dome microcavity. The physical properties of these devices are discussed in the following section.

Droplet acoustics measurements were performed by manually placing ethylene glycol droplets directly on top of the device using a 30-gauge needle. Precise placement was enabled by both top- and side-view cameras. Droplet breathing modes induced by thermal Brownian motion resulted in acoustic pressure waves that coupled into the system by deflecting the top Bragg mirror which shifted the cavity resonance and created a time-varying signal that could be readout by the photodetector. All measurements were taken using an 80 MHz sampling rate averaged over 300 samples. Optical powers for interrogation and collection were on the order of 1 mW and 50 μW, respectively. The power spectral density traces displayed here as well as in the main text were smoothed with 200-point averaging.

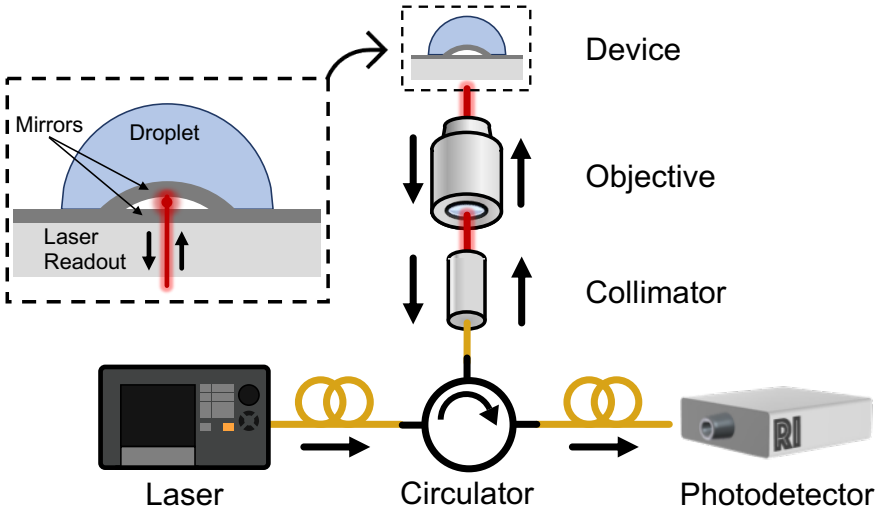

Supplementary Figure 1. Schematic representation of the experimental setup. A tunable laser (Santec TSL-710) was connected to an optical circulator. The beam was collimated (Thorlabs RC08APC-P01) and focused through the back of the quartz substrate onto the device using a microscope objective. Reflected light was directed back into the circulator and passed to a photodetector (Resolved Instruments DPD80). External vibrations deflect the upper buckled mirror, which in turn generates a time-based optical signal.

2 Optical and mechanical properties of buckled dome microcavities

We have previously published multiple studies on the optical properties of buckled dome microcavities [1,4,5] but have also included a discussion here for easy reference. An optical transmission scan of a representative device is shown in Fig. S.2(a). These devices possess Laguerre-Gaussian and Hermite-Gaussian modes (as shown in the inset photographs assigned to the transmission peaks) characteristic of a spherical mirror cavity, and their spectral and spatial properties are determined by the length of the partially evacuated airgap separating the two Bragg mirrors as well as the curvature of the buckled top mirror. Figure S.2(b) shows a microscope colour image of an array of 100 µm-diameter buckled dome microcavities.

Our mechanical measurement scheme utilizes a 'tuned-to-slope' technique where the interrogation laser is slightly detuned from the fundamental optical resonance shown in Fig. S.2(a). This allows slight deviations in cavity length caused by incoming pressure waves to couple to the optical system in the form of a time-based signal which is then converted to the frequency domain. It is also important to note that the external environment can impact the position and amplitude of the mechanical modes of the buckled microcavity devices. Power spectral density plots for a typical device covered by bulk air and bulk ethylene glycol media are shown in Fig. 2(c) and Fig. 2(d), respectively, demonstrating the effect that the external medium has on the thermomechanical properties of the sensor. When submerged in ethylene glycol, the mechanical modes shift to lower frequencies and exhibit increased damping.

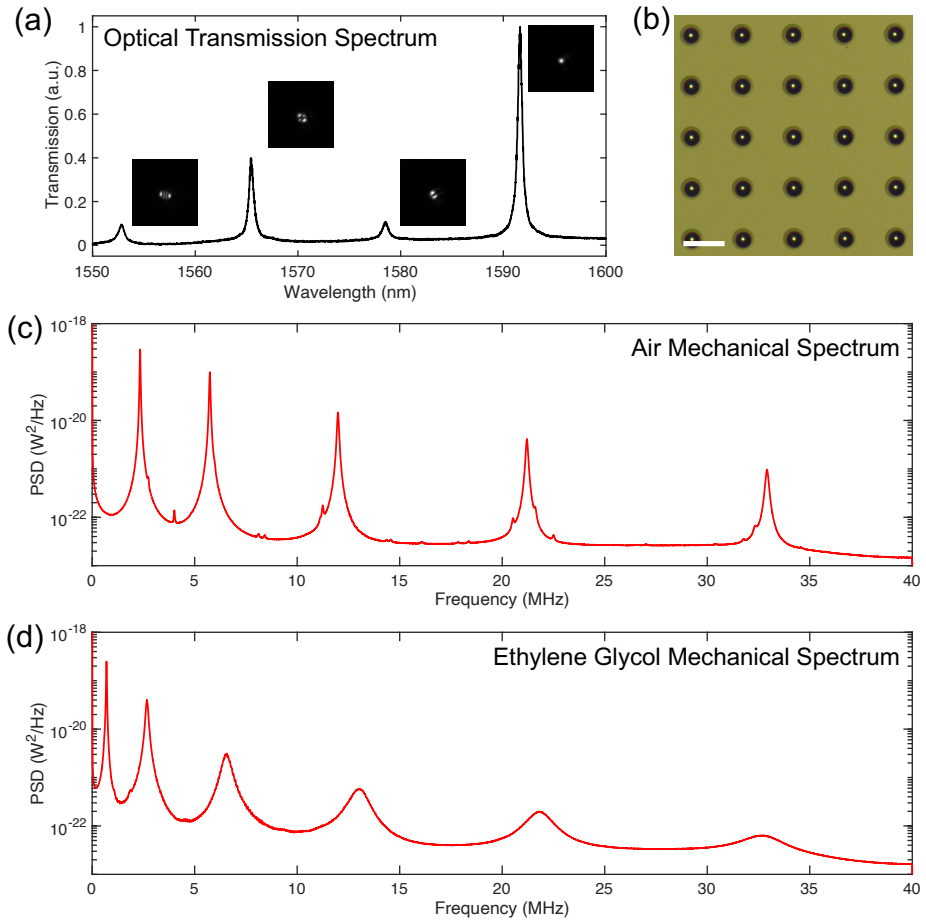

Supplementary Figure 2. Optical and mechanical properties of buckled dome microcavities. (a) A representative optical transmission scan for a 100 µm diameter device showing a family of optical modes. Camera images have also been included for each mode. (b) A microscope image of a 5-by-5 array of 100 µm-diameter buckled dome microcavities. Scale bar – 200 µm. (c) A representative mechanical spectrum showing the mechanical modes of a cavity in air. d) A representative mechanical spectrum showing the mechanical modes of a cavity submerged in ethylene glycol.

3 Numerical simulations of droplet acoustics

Numerical simulations of the droplet acoustics were performed with the pressure acoustics module in COMSOL Multiphysics. The speed of sound in ethylene glycol was set to 1660 m/s and the density was set to 1100 mg/m^3 [6-7]. Each droplet was modelled as a spherical cap using estimated dimensions (i.e., radius and height) obtained from top- and side-view camera images. In each case, the approximation was made that the droplet was centered on the sensor. A 'soft sound boundary' was used to model the droplet-air interface, as well as the droplet-sensor interface. This boundary condition sets the pressure to zero at the interface and is appropriate for the droplet-sensor interface since the upper mirror of the sensor can be modelled as a flexible membrane. This distinction becomes increasingly important with decreasing droplet size. A 'hard sound boundary' was used at the droplet-substrate interface (i.e., outside the dimeter of the sensor), which holds the normal component of the velocity and acceleration at zero. A representative geometry showing the various boundaries is shown in Fig. S.3. Discrete eigenfrequencies and their corresponding acoustic pressure distributions were extracted from the model, which can be seen throughout the main text.

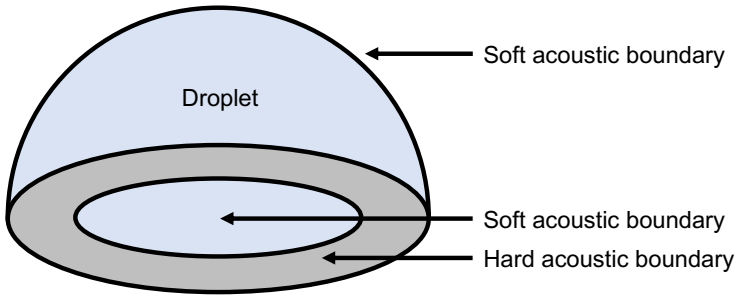

Supplementary Figure 3. Boundary conditions used in numerical simulations. In addition to the droplet-air interface, a soft acoustic boundary was used where the droplet was in contact with the sensor to account for the membrane-like behavior of the buckled top mirror.

4 Additional droplet results

To augment droplet results presented in the main text, results for several additional droplets are presented below in S.4. The black arrows denote the first resonance assigned to each droplet and show a clear trend in frequency versus droplet size. The vibrational spectrum for each droplet is plotted against a measurement taken in bulk ethylene glycol to show the location of features intrinsic to the buckled dome microcavity. We have also included additional droplet evaporation results for a droplet that was initially well-centered in Fig. S.5. Dimensions of all droplets studied are provided in Table S.1 along with experimental resonance frequencies and the corresponding quality factors. We noted that the size of the droplet also impacted the position of the dome mechanical modes in frequency-space, and that the modes were shifted to slightly higher frequencies for smaller droplets due to the decreased loading applied to the top Bragg mirror. In some cases, Fano resonance features are observed due to the hybridization of device modes with droplet modes, which is consistent with previous observations[2].

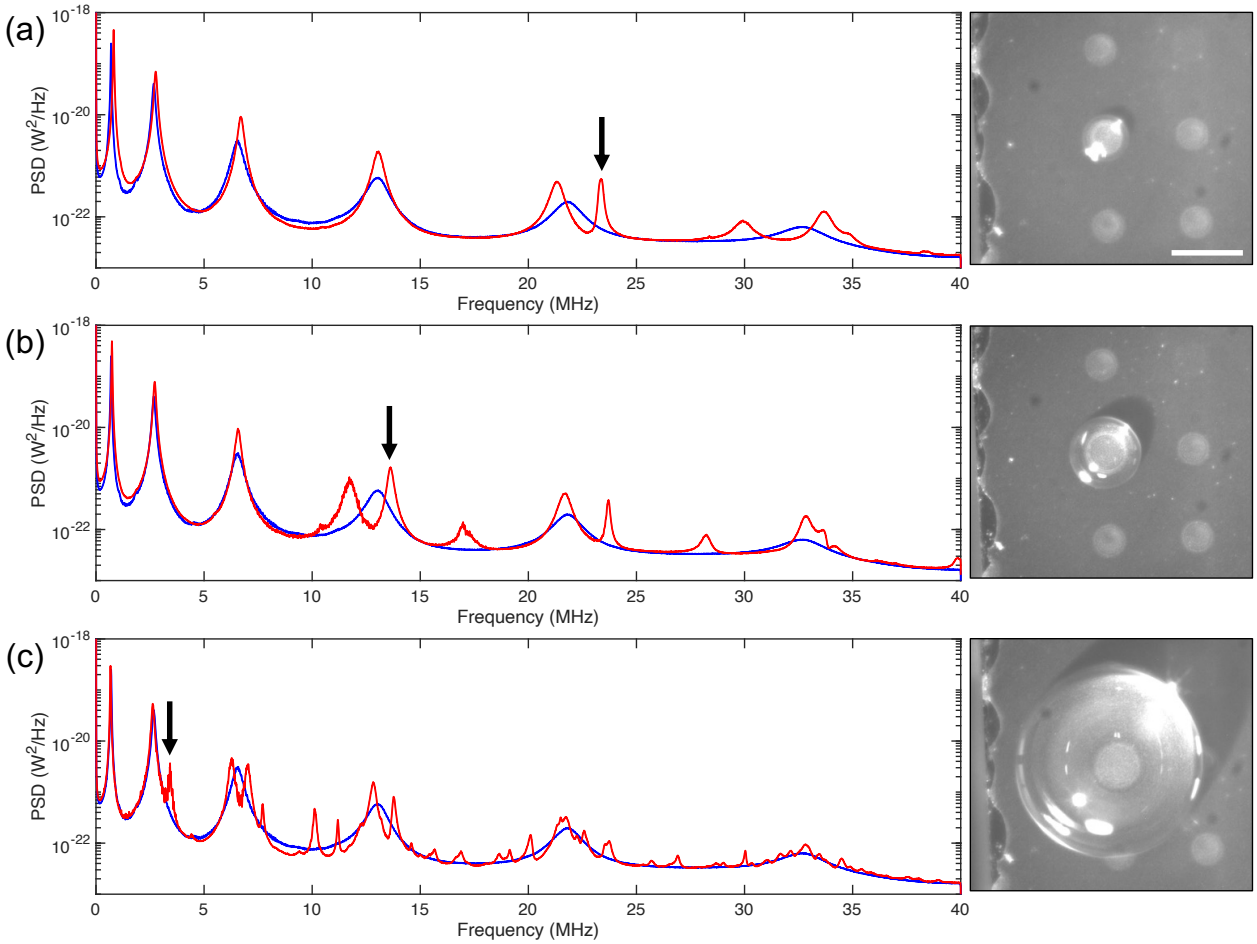

Supplementary Figure 4. Additional droplet results (red) compared against bulk ethylene glycol measurements (blue). (a) Results for a droplet with a radius of 66 µm and a height of 42 µm. A top-down view of the droplet has also been included. Scale bar – 200 µm. (b) Results for a droplet with a radius of 100 µm and a height of 77 µm. (c) Results for a droplet with a radius of 263 µm and a height of 268 µm. The black arrows correspond to the first mode for each droplet.

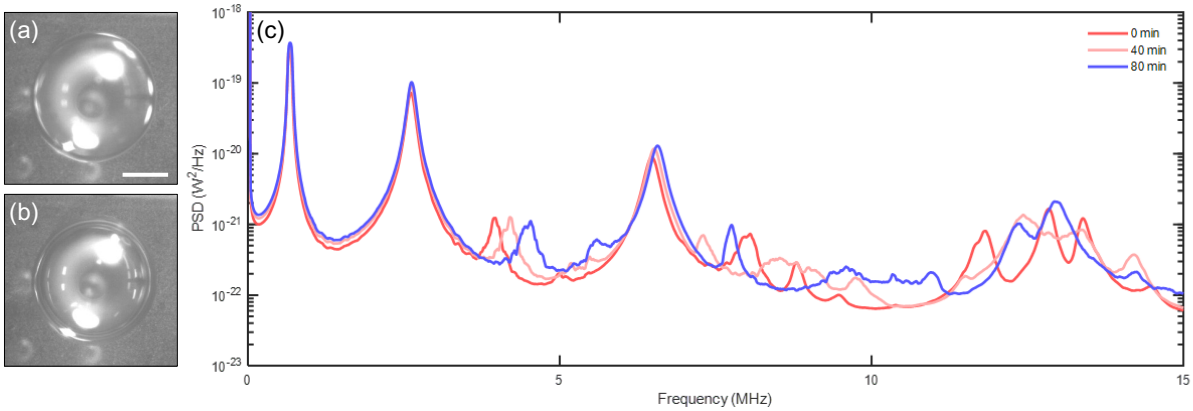

Supplementary Figure 5. Additional droplet evaporation results with better initial alignment. (a-b) Top-down views of the droplet after 0 minutes and 80 minutes, respectively. Scale bar – 200 µm. (c) Power spectral densities of the evaporating droplet analogous to the results shown in Fig. 5 of the main text.

Supplementary Table 1. Droplet dimensions and resonance characteristics. The Q factor is generally on the order of 10^2 with the smallest, well-centered droplets possessing the highest values.

Droplet	Radius (µm)	Height (µm)	Lowest Mode (MHz)	Q Factor
A	122	106	9.36	35
B	100	77	13.62	30
C	144	136	7.33	26
D	147	133	7.28	23
E	101	68	14.00	23
F	84	60	20.58	23
G	125	112	8.80	14
H	105	74	13.74	30
I	70	45	22.84	85
J	66	42	23.36	93
K	241	248	3.76	54
L	246	262	3.65	37
M	344	368	2.83	22
N	263	268	3.46	-
O	206	209	4.40	55

References:

[1] G. J. Hornig, K. G. Scheuer, E. B. Dew, R. Zemp and R. G. DeCorby, *Optics Express,* 2022, **30**, 33083.

[2] G. J. Hornig, K. G. Scheuer and R. G. DeCorby, *arXiv*, 2023.

[3] K. G. Scheuer and R. G. DeCorby, *Sensors*, 2023, **23**, 5665.

[4] C. A. Potts, A. Melnyk, H. Ramp, M. H. Bitarafan, D. Vick, L. J. LeBlanc, J. P. Davis and R. G. DeCorby, *Applied Physics Letters*, 2016, **108**, 041103.

[5] G. J. Hornig, L. Bu, S. Al-Sumaidae and R. G. DeCorby, *JOSA B*, 2022, **39**, 884.

[6] A. Goldstein and L. N. Langrill, *J. Clin. Ultrasound*, 1979, **7**, 465.

[7] E. T. Fogg, A. Norman Hixson, and R. Thompson, *Anal Chem*, 1955, **27,** 1609.